Front. For. China 2007, 2(1): 72–77
DOI 10.1007/s11461-007-0011-6

RESEARCH ARTICLE

WANG Yujie, WANG Yunqi

Impacts of fractal features of soil on moisture infiltration capacity of typical stands in Jinyun mountain of Chongqing city

© Higher Education Press and Springer-Verlag 2007

Abstract The soil structure was expressed with fractal dimensions of particle size distribution (PSD), aggregate size distribution (ASD), and soil pore size distribution (SPD). The effect of soil fractal features on soil infiltration velocity and process was studied. The result of the fractal feature shows that fractal dimensions of PSD are obviously greater than those of ASD and SPD, and in different soil genetic horizons, the fractal dimension of ASD has the greatest variability, and shows a downtrend on the top-to-bottom genetic horizon. According to the soil infiltration process curve, the infiltration process was divided into three phases: (1) the initial phase (0–5 min), (2) the transition phase (5–30 min), and (3) the stable phase (30–180 min). In the initial phase of infiltration, the soil structure of soil genetic horizon A was the major influencing factor; in the transition phase of infiltration, the pore distribution of soil horizon AB and soil structure of horizon B were the major influencing factors; in the stable phase of infiltration, the soil structure of horizon C was the major influencing factor to the infiltration velocity. Soil infiltration process is influenced comprehensively by soil PSD, ASD, and SPD. In the overall soil water infiltration, the infiltration in shrub forest land was much faster than that in other land uses, and in the initial infiltration phase, arable land soil infiltration was much faster than that in forest land, and in the stable infiltration phase, the infiltration velocity in forest land was faster than that in arable land.

Keywords infiltration process, soil structure, fractal feature, fractal dimension

Translated from *Journal of Beijing Forestry University*, 2006, 28(3): 73–78 [译自: 北京林业大学学报]

WANG Yujie (✉), WANG Yunqi
Key Laboratory of Soil and Water Conservation and Desertification Combating, Ministry of Education, College of Soil and Water Conservation, Beijing Forestry University, Beijing 100083, China
E-mail: wyujie@bjfu.edu.cn

1 Introduction

Soil comprises water, air, and solid particles with varied directions and shapes. Connectivity has a great impact on liquid and its movement characteristics in solid particles. The array forms, sizes, and shapes of solid ingredients and interstices constitute soil structure and determine the series of characteristics and diversification of soil physics properties. Moisture movement in soil is a quite complex issue. Therefore, the soil moisture infiltration process is closely associated with soil particle size distribution and soil pore size distribution.

Since the 1980s, fractal theory has been applied to soil research, which makes it possible to quantitatively describe complex soil characteristics; it offers a reliable parameter and theory to illustrate soil hydraulics characteristics and shows up and simulates soil moisture distribution rules. Consequently, the fractal dimensions of particle size distribution (PSD) and aggregate size distribution (ASD) were described by particle size weight distribution (Tyler and Wheatcraft, 1992; Yang et al., 1993; Bird et al., 1996; Wu and Hong, 1999). The fractal dimension of soil pore was represented by soil pore size distribution (SPD) (Tyler and Wheatcraft, 1989, 1990, 1992; Rieu and Sposito, 1991; Pefect et al., 1996).

Jinyun mountain in Chongqing city is located at the tail of the Three Gorges Reservoir Areas. The forest overall comprises subtropical evergreen broadleaved trees, generally represents the natural background of subtropical forest ecosystem, and has been a natural laboratory of forest functions in water holding and flood controlling. In this study, soil structure was expressed by the fractal dimension of soil particle size (SPD) and aggregate size distribution based on Katz method (Wu and Hong, 1999) and the fractal dimension of soil pore size distribution (SPD) was expressed based on Menger sponge structure (Huang and Zhan, 2002). We try to study further the influence of fractal features of soil on moisture infiltration in typical forestlands, and provide some bases for the Three Gorges Reservoir Areas vegetation construction with water regulation and flood control.

2 Study area

The study site (29°45′ N, 106°22′ E) is in the Jinyun Mountain, National Nature Reserve, in Small Three Gorges in the Jialing river, with the highest elevation at 951.5 m and relative elevation variation at 600 m, and is covered mostly by yellow soil (pH 4.0–4.5) and paddy soil. It belongs to the typical evergreen broadleaved forest bioclimatic horizontal zone of subtropical belt with the mean annual temperature of 13.6°C, precipitation 1,611.8 mm, and evaporation capacity 777.1 mm, and is greatly rich in plant resources. There are six major vegetation types: evergreen broadleaved forest, warm coniferous forests, bamboo grove, evergreen broadleaved shrubs, subtropical shrubs, hassock, and aquatic plants. The main dominant plant species are *Pinus massoniana, Cunninghamia lanceolata, Castanopsis fargesil, Pinus armandii, Boletus edulis, Gordonia acuminata*, and *Symplocos setchuanensis*.

In this study site, the plots of the four typical stands (mixed conifer-broadleaf forest, evergreen broadleaved forest, bamboo grove, and evergreen broadleaved shrub) were taken to study the structure influence on moisture infiltration in soil and the arable land was taken as the control plot. The basic information on stands is shown in Tables 1 and 2.

3 Research methods

3.1 Fractal dimensions of PSD and ASD

Soil particle distribution fractal feature model created by Yang (1993) was adopted to calculate the fractal dimensions of PSD and ASD. Soil is a porous medium with self-similar structure; the soil volume weight of particles with greater diameter than a particle one $d_i (d_i > d_{i+1}, i = 1,2,\ldots)$ is $W(\delta > d_i)$:

$$1-(\bar{d}_i/\bar{d}_{\max})^{3-D} = W(\delta > \bar{d}_i)/W_0 \quad (1)$$

where $\bar{d}_i$ is the average value of d_i and d_{i+1} $(d_i = (d_i + d_{i+1})/2)$, $\bar{d}_{\max}$ is the average value of maximum diameter grade, $W(\delta \geqslant \bar{d}_{\max}) = 0, W(\delta > \bar{d}_i)$, is the cumulative weight greater than $\bar{d}_i$, and W_0 is the total weight value.

Take $\lg(W_i/W_0)$ and $\lg(\bar{d}_i/\bar{d}_{\max})$ as longitudinal and horizontal ordinate, so the $3-D$ is the rate of grade, then D is the fractal dimension calculated by regression. D_P is defined as the fractal dimension of PSD and D_A is the fractal dimension of ASD. The calculation results are shown in Table 3.

Pipette method was used to measure the individual particle size weight of PSD and ASD (Shen et al., 2000).

3.2 The fractal dimension of SPD

Soil water retention characteristic curve model, created by Huang based on Menger sponge structure, was selected to calculate the fractal dimension of SPD (Huang and Zhan, 2002):

$$\frac{\theta}{\theta_s} = \left[\frac{\psi}{\psi_a}\right]^{D-3} \quad (2)$$

where D is the fractal dimension of SPD; θ is water content; θ_s is saturation water content; ψ is matrix suction; and ψ_a is air-entry suction.

Table 1 Basic information on typical stands standard land in Jinyun mountain

Stands	Site factor			Stand information					Litter	
	Elevation /m	Aspect	Slope gradient /(°)	Origin	Age class	Canopy density	Underwood coverage /%	Ground coverage /%	Depth /cm	Storage /(t·hm^{-2})
Mixed conifer-broadleaf forest	760	N-W	16–25	Natural	VI	0.9	40	30	3.5	31.57
Evergreen broadleaved forest	825	N-W	26	Natural	VI	0.9	40	20	3.4	58.90
Bamboo grove	800	N-W	11	Natural	V	0.85	10	80	1.4	29.11
Evergreen broadleaved shrub	860	N-W	10	Natural	V	0.95	60	50	4.5	86.85

Table 2 Basic makeup of typical stands in Jinyun mountain

Stands	Tree species	Undergrowth planting species	Herbaceous species
Mixed conifer-broadleaf forest	*Gordonia acuminate*, *Pinus massoniana*, *Symplocos setchuensis*, *Adinandra bockiana*	*Eurya japonica*, *Adinandra bockiana*, *Symplocos lancifolia*, *Neolitea aurata*, *Diospyros morrisiana*	Pteridiaceae, *Woodwardia japonica*, *Diplopterygium glauca*, *Lophatherum gracile*
Evergreen broadleaved forest	*Gordonia acuminate*, *Neolitea aurata*, *Adinandra bockiana*	*Castanopsis carlesii*, *Rhamnus esquirolii*, *Symplocos setchuensis*, *Eurya japonica*	Pteridiaceae, *Woodwardia japonica*, *Lophatherum gracile*
Bamboo grove	*Phyllostachys pubescens*	*Mells indica*, *Smilax china*, *Ficus virens*	Pteridiaceae, *Pilea pumila*, *Oplismenus compositus*, *Commelina communis*, *Viola tricolor*
Evergreen broadleaved shrub	*Alniphyllum fortunei*, *Lindera. kwangtunensis*, *Neolitea aurata*, *Symplocos caudate*	*Cunninghamia lanceolata*, *Eurya japonica*, *Elaeocarpus japonicus*, *Machilus nanmu*, *Camellia japonica*	Pteridiaceae, *emercocallis fulva*, *Crassocephalum rabens*, *Conyza Canadensis*

Table 3 Soil structure features, organism content, and soil water stable permeability

Soil horizon	Stand	ASD		PSD		SPD		Organic content C /(g·kg^{-1})	Final infiltration capacity /(cm·min^{-1})
		D_A	R_A	D_P	R_P	D_{SP}	R_{SP}		
A	Mixed conifer-broadleaf forest	2.713	0.980	2.844	0.956	2.678	0.902	46.2	1.570
	Evergreen broadleaved forest	2.714	0.969	2.827	0.956	2.652	0.849	31.8	1.575
	Bamboo grove	2.630	0.995	2.735	0.984	2.567	0.926	20.8	16.200
	Evergreen broadleaved shrub	2.644	0.982	2.878	0.961	2.811	0.981	77.9	7.143
	Arable land	2.728	0.953	2.874	0.924	2.747	0.949	69.7	16.220
AB	Mixed conifer-broadleaf forest	2.644	0.904	2.871	0.921	2.645	0.889	6.9	0.073
	Evergreen broadleaved forest	2.654	0.978	2.810	0.996	2.641	0.928	3.0	0.084
	Bamboo grove	2.680	0.990	2.778	0.995	2.485	0.988	11.0	0.036
	Evergreen broadleaved shrub	2.510	0.930	2.829	0.836	2.799	0.944	14.1	2.368
	Arable land	2.674	0.913	2.853	0.853	2.669	0.919	9.1	0.023
B	Mixed conifer-broadleaf forest	2.645	0.938	2.863	0.991	2.699	0.941	3.9	0.028
	Evergreen broadleaved forest	2.644	0.981	2.764	0.993	2.684	0.966	0.8	0.029
	Bamboo grove	2.679	0.993	2.771	0.990	2.371	0.835	3.2	0.015
	Evergreen broadleaved shrub	2.592	0.977	2.747	0.966	2.747	0.951	2.9	1.025
	Arable land	2.746	0.939	2.867	0.974	2.638	0.897	3.0	0.002
C	Mixed conifer-broadleaf forest	2.664	0.986	2.794	0.995	2.321	0.986	1.2	0.055
	Evergreen broadleaved forest	2.684	0.973	2.805	0.992	2.459	0.904	1.0	0.051
	Bamboo grove	2.660	0.958	2.797	0.996	2.442	0.875	2.0	0.055
	Arable land	2.725	0.968	2.813	0.992	2.585	0.960	1.4	0.007

Soil water retention characteristic curve is fitted using power function to capture the power value of $1/(D-3)$; D is the fractal dimension of SPD and D_{SP} is calculated (see Table 3).

Pressure membrane method was used to measure soil water retention characteristic curve.

3.3 Soil moisture infiltration

Simulated infiltration rate of soil moisture was adapted to the following.

The Phillip infiltration equation:

$$f = \frac{1}{2} s t^{-\frac{1}{2}} + A \tag{3}$$

where s is the sorptivity of the soil and A is a final infiltration capacity.

The Horton infiltration equation:

$$f = f_c + (f_0 - f_c)e^{-kt} \tag{4}$$

where f_c is the final infiltration capacity, f_0 is the initial infiltration capacity, and k is an empirical coefficient.

Power function regression:

$$f = at^{-b} \tag{5}$$

where a, b are empirical coefficients.

Selecting the optimal infiltration model according to the regression coefficient value, the result is shown in Table 4.

Double-ring permeation was used to measure the real infiltration process in the field, and undisturbed soil final infiltration rate of each genetic horizon was measured by the cutting ring.

Table 4 Infiltration models of typical forest stands

Stands	Infiltration model	R
Mixed conifer-broadleaf forest	$f = \frac{1}{2} \times 6.711\, t^{-\frac{1}{2}} + 0.347$	0.947
Evergreen broadleaved forest	$f = \frac{1}{2} \times 3.242\, t^{-\frac{1}{2}} + 0.407$	0.991
Bamboo groves	$f = \frac{1}{2} \times 10.196\, t^{-\frac{1}{2}} + 0.429$	0.987
Evergreen broadleaved shrubs	$f = \frac{1}{2} \times 25.010\, t^{-\frac{1}{2}} + 9.200$	0.969
Arable land	$f = 0.253 + 18.156\, e^{-0.0606\, t}$	0.978

Considering the influence of organic content on infiltration rate, potassium dichromate method was used to measure organic content.

4 Results and analyses

4.1 Fractal features of typical forest land soil

For soil PSD, the lighter the soil texture, the greater the fractal dimension value. The dimension of PSD was 2.735–2.878, and the maximal fractal dimension of PSD was in arable land (2.823–2.874) with the lightest soil texture; moreover, the minimal was in the bamboo grove (2.735–2.797) with the heaviest soil texture (in Table 3)

The dimension value of ASD indicates influences of soil aggregate content on soil structure and stability. That is the smaller the dimension value, the better the soil structure and stability. The value of fractal dimension of ASD was 2.510–2.746. The fractal dimension of PSD was obviously greater than that of ASD. Accordingly both the activity of the forest and the activity arable land have positive effects on optimal

soil structure. The soil fractal dimension value of ASD was minimal (2.510–2.644) in evergreen broadleaved shrubs and the maximal (2.674–2.746) in arable land. The results show that the best soil structure and stability was observed in the shrub soil, and the soil structure of arable land was worse than that of forestland.

The greater the fractal dimension value of SPD, the better the soil porosity connectivity. However, the soil porosity connectivity is worse due to small and non-homogeneous pores. The value of the fractal dimension of SPD (2.321–2.799) showed greater variation in each soil horizon than that of fractal dimensions of PSD and ASD, especially in mixed conifer-broadleaf forest (2.321–2.699) and evergreen broad-leaved forest (2.459–2.684). The greatest fractal dimension value of SPD was found in evergreen broad-leaved shrubs; therefore, homogeneous soil porosity and connectivity are good. The arable land was the second favorable soil type, which contributed to direct human positive activities, and the worst was the bamboo grove.

4.2 Impacts of fractal features on moisture infiltration capacity of soil

4.2.1 Soil moisture infiltration process

According to the related correlation R value of different infiltration model simulations, the Philip equation was optimal to forest land soil and Horton equation was best to arable land soil. Generally, the infiltration model was better than the power function regression. The soil moisture infiltration model of different stands and arable land is shown in Table 4, and the infiltration simulation process is given in Fig. 1. Soil moisture infiltration capacity of evergreen broadleaved forest was dramatically greater than that of other stands and arable land. The initial infiltration capacity of arable land was relatively greater, while the final infiltration capacity was much smaller than that of other stands (Fig. 1).

The soil moisture infiltration in the initial 180 min was simulated based on the infiltration model demonstrated in Table 4 and Fig. 1. The infiltration process can be divided into three phases: (1) the initial phase (0–5 min), (2) the transition phase (5–30 min), and (3) the stable phase (30–180 min), to study the influence of structure on moisture infiltration in soil.

4.2.2 The impacts in the initial phase $t(\min) = [0, 5]$

In the initial infiltration phase $t(\min) = [0, 5]$, the result of regression of f and D_{P}, D_{A}, D_{SP}, is as follows:

$$f = -1.324\,t + 416.870\,D_{\mathrm{SPA}} - 605.952\,D_{\mathrm{PA}} + 199.610\,D_{\mathrm{AA}} + 71.126,\ R = 0.957,\ t(\min) = [0,5] \quad (6)$$

Equation (6) shows, within the initial 5 min, with the fastest reduction of infiltration capacity, the infiltration capacity was directly affected by the fractal dimensions of the PSD, ASD, and SPD. In the initial 5 min the infiltration capacity was dominated by the structure of soil horizon A. In this phase, infiltration capacity had positive correlation with D_{SP} and D_{A}, and had negative correlation with D_{P}. In this equation, coefficients of each fractal dimension were the same order of magnitude. This means that the initial infiltration capacity was synthetically influenced by PSD, ASD, and SPD; moreover, the effects of PSD and SPD were greater than that of ASD.

Figure 1 indicates that in the initial 5 min, the infiltration capacity of evergreen broadleaved shrub and arable land was much greater that of other stands, which can be directly explained by the greatest fractal dimension (2.811, 2.747). In other words, good pore connectivity increased its permeability. The infiltration capacity of the bamboo grove is slightly higher than that of mixed conifer-broadleaf forest and evergreen broadleaved forest due to the coarse texture with a highly small fractal dimension value of PSD (2.735).

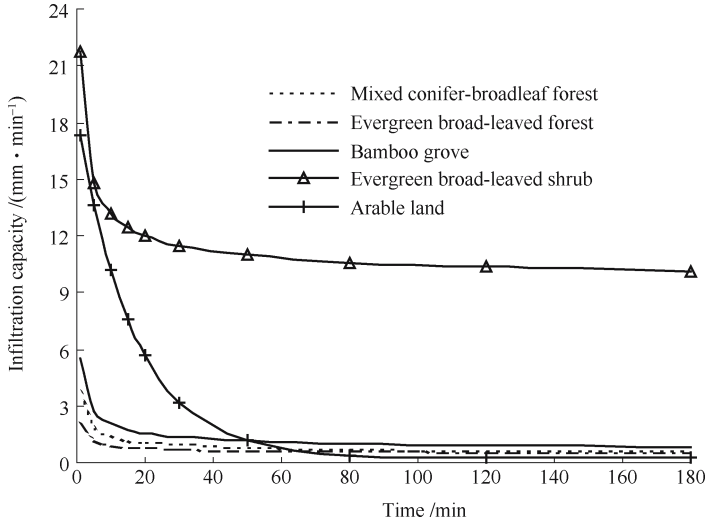

Fig. 1 The soil water infiltration process of typical stands in Jinyun mountain

4.2.3 The influences in the transition phase $t(\min) = (5, 30)$

In the transition phase $t(\min) = (5, 30)$, the infiltration capacity became slow and was influenced by SPD of soil genetic horizons AB and B, and PSD and ASD of soil horizon B. Regression equation (7) indicates that the coefficient of D_{SPAB} (93.167) and D_{SPB} (−48.713) was one order of magnitude higher than the others; hence the SPD, especially the SPD of AB soil genetic horizon, had the greatest influence on the infiltration in this phase.

$$f = -0.097\,t + 93.167\,D_{SPAB} - 48.713\,D_{SPB} + 6.465\,D_{PB} + 2.078\,D_{AB} - 136.011,\ R = 0.979,\ t(\min) = (5, 30) \quad (7)$$

Figure 1 shows that soil moisture infiltration capacity of evergreen broadleaved shrub is much larger than that of others, which is induced by the maximal fractal dimension value of SPD (2.799) of soil genetic horizon AB. However, the quick reduction in soil moisture infiltration capacity of arable land responds to the fast changing fractal dimension value from soil genetic horizon A (2.747) to horizon AB (2.669). As a result, the inferior connectivity intended to decline the infiltration capacity of soil in this phase.

4.2.4 The influence in the stable phase $t(\min) = (30,180)$

The regression equation (8) indicates that in the stable phase $t(\min) = (30,180)$ the infiltration capacity was dominated by the structure of soil genetic horizon C (the B soil horizon of evergreen broadleaved shrub). In the stable phase, the magnitude order of coefficients of D_{PC} (−144.737) was one greater than that of D_{SPC} and D_{AC}, which also means that the structure of soil horizon C cannot be easily disturbed by external environment.

$$f = -0.003\,t + 8.269\,D_{SPC} - 144.737\,D_{PC} + 6.845\,D_{AC} + 368.000,\ R = 0.998,\ t(\min) = (30,180) \quad (8)$$

There is no soil horizon C in evergreen broadleaved shrubs, so the structure of soil horizon B was still taken into account in the stable phase.

The maximal infiltration capacity was constant in evergreen broadleaved shrubs and minimum in arable land, which is shown in Fig. 1. It is directly related to the shrub's minimal (2.747) and arable land's maximal (2.813) fractal dimension value of PSD.

4.2.5 The impacts of structure on final infiltration capacity of each soil genetic horizon

The final infiltration capacities of each soil horizon were measured with cutting ring. Soil organic matter is both porous matter and cementing agent, and hence it has predominant influence on soil porosity. The influence of organic matter on soil structure can be ignored since the infiltration process in the field was conducted using the double-ring permeation. However, undisturbed soil cutting with cutting ring is small; as a consequence, the organic matter's influence cannot be ignored.

The regression result of the final infiltration capacity with the fractal dimension value of PSD, ASD, SPD, and organic matter (C) is given by Eq. (9).

$$f^{1/2} = 0.852D_{SP} - 11.647D_{P} - 2.972D_{A} + 0.525C + 38.614,\ R = 0.849 \quad (9)$$

Equation (9) shows that the higher the fractal dimension of PSD, the lighter the soil texture, and the slower the final infiltration capacity. It also means the higher the fractal dimension of SPD, the more homogeneous the soil porosity; the smaller the fractal dimension of ASD, the better the aggregation; and the higher the organic content, the faster the final infiltration capacity.

4.3 The impacts of fractal features of soil structure on the infiltration process

From Eqs. (6), (7), and (8), it can be concluded that the influence of infiltration capacity decreases with time, the coefficients of time descending three order of magnitudes from 1.324 to 0.003. The whole infiltration process has little relation to the PSD and ASD of soil horizon AB. The final infiltration capacity of soil horizon AB was far lower than that of horizon A, so the soil water could filter into soil horizon AB from A with higher velocity, and then move into B with relative lower velocity.

Normally, in the whole infiltration process, the infiltration capacity of evergreen broadleaved shrub is much better than that of other forest and arable lands, which can be explained by its optimal soil structure. The infiltration capacity of arable land is greater than that of other forests in the initial and transition phases. This is the reason why good upper soil structure contributed to positive human activities. However, in the stable phase, the infiltration capacity of forest land is faster than that of arable land due to the deep forest plants improving the lower soil structure.

5 Conclusions

1) In the Jinyun Mountain, the Three Gorges Reservoir Areas, the fractal dimension of PSD was largely higher than that of ASD. The order of fractal dimension of PSD is given as follows: bamboo grove < evergreen broadleaved forest < evergreen broadleaved shrub < mixed conifer-broadleaf forest < arable land. The order of fractal dimension of ASD is given as follows: evergreen broadleaved shrub < bamboo grove < mixed conifer-broadleaf forest, evergreen broadleaved forest < arable land. The order of fractal dimension of SPD is given as follows: broadleaved shrub > mixed coniferbroadleaf forest, evergreen broadleaved forest > bamboo grove > arable land. The evergreen broadleaved shrub has the best soil structure.

2) In the initial phase (0–5 min), the infiltration capacity was influenced by the structure of soil genetic horizon A. The soil moisture infiltration capacity of evergreen broadleaved shrub and arable land was far greater that of other forests.

3) In the transition phase (5–30 min), the SPD of soil horizons AB and B, and the PSD and ASD of horizon B had great impacts on infiltration capacity. The infiltration capacity of evergreen broadleaved shrub was still the highest, while the arable land soil moisture infiltration reduced quickly.

4) In the stable phase (30–180 min), the infiltration capacity was dominated by the structure of soil horizon C. The PSD had the most negative influence on infiltration capacity. The infiltration capacity of evergreen broadleaved shrubs was still the highest, while the infiltration capacity of arable land reduced to less than that of other forests.

5) The higher the fractal dimension of PSD, and the lighter the soil texture, the slower the final infiltration capacity. The higher the fractal dimension of SPD, the more homogeneous the soil porosity; the smaller the fractal dimension of ASD, the better the aggregating; and the higher the organic content, the faster the final infiltration capacity.

Acknowledgements This study was supported by the National Natural Science Foundation of China (Grant No. 30671661).

References

Bird N R H, Bartoli F, Dexter A R (1996). Water retention models fro fractal soil structures. Eupr J Soil Sci, 47: 1–6

Huang G H, Zhan W H (2002). Modeling soil water retention curve with fractal theory. Adv Water Sci, 13(1): 55–60 (in Chinese)

Pefect E, Mchaughlin N B, Kay B D, Topp G C (1996). An improved fractal equation for the soil water retention curve. Water Resour Res, 32: 281–287

Rieu M, Sposito G (1991). Fractal fragmentation, soil porosity and soil water properties I. Application. Soil Sci Soc Am J, 55: 1,231–1,238

Shen H, Jiang F Q, Du X J (2000). Evaluation on soil anti-erodibility of soil and water conservation forest. Chin J Appl Ecol, 11(3): 345–348 (in Chinese)

Tyler S W, Wheatcraft S W (1989). Application of fractal mathematics to soil water retention estimation. Soil Sci Soc Am J, 53: 987–996

Tyler S W, Wheatcraft S W (1990). Fractal processes in soil water relation. Water Resour Res, 26(5): 1,047–1,054

Tyler S W, Wheatcraft S W (1992). Fractal scaling of soil particle size distributions: analysis and limitations. Soil Sci Soc Am J, 56: 362–369

Wu C Z, Hong W (1999). Study on fractal features of soil aggregate structure under different management patterns. Acta Pedol Sin, 36(2): 162–167 (in Chinese)

Yang P L, Luo Y P, Shi Y C (1993). Fractal features of soil characterized by particle weight distribution. Chin Sci Bull, 38(20): 1,896–1,899 (in Chinese)